Sum frequency and second harmonic generation from the surface of a liquid microjet

Nikolay Smolentsev, Yixing Chen, Kailash C. Jena, Matthew A. Brown, and Sylvie Roke

---

Articles you may be interested in

"Half-hydration" at the air/water interface revealed by heterodyne-detected electronic sum frequency generation spectroscopy, polarization second harmonic generation, and molecular dynamics simulation
J. Chem. Phys. **132**, 144701 (2010); 10.1063/1.3372620

Origin of second harmonic generation optical activity of a tryptophan derivative at the air/water interface
J. Chem. Phys. **125**, 044716 (2006); 10.1063/1.2216696

Detection of flexoelectric effect from 4-heptyloxy- 4 ′ -cyanobiphenyl monolayers at an air-water interface by Maxwell displacement current and optical second harmonic generation
J. Chem. Phys. **122**, 164703 (2005); 10.1063/1.1884597

Second-harmonic generation and Maxwell displacement current spectroscopy of chiral organic monolayers at the air–water interface
J. Chem. Phys. **119**, 7427 (2003); 10.1063/1.1605943

Orientational order study of monolayers at the air–water interface by Maxwell-displacement current and optical second harmonic generation
J. Chem. Phys. **115**, 9010 (2001); 10.1063/1.1413738

Sum frequency and second harmonic generation from the surface of a liquid microjet

Nikolay Smolentsev,[1] Yixing Chen,[1] Kailash C. Jena,[1,2] Matthew A. Brown,[3] and Sylvie Roke[1,a)]

[1]*Laboratory for Fundamental Biophotonics (LBP), Institute of Bioengineering (IBI), School of Engineering (STI), École Polytechnique Fédérale de Lausanne (EPFL), 1015 Lausanne, Switzerland*
[2]*Department of Physics, Indian Institute of Technology Ropar, Rupnagar, 140001, India*
[3]*Laboratory for Surface Science and Technology, Department of Materials, ETH Zürich, CH-8093 Zurich, Switzerland*

The use of a liquid microjet as a possible source of interest for Second Harmonic Generation (SHG) and Sum Frequency Generation (SFG) spectroscopy is examined. We measured non-resonant SHG scattering patterns from the air/water interface of a microjet of pure water and observe a strong enhancement of the SHG signal for certain scattering angles. These enhancements can be explained by the optical properties and the shape of the liquid microjet. SFG experiments at the surface of a liquid microjet of ethanol in air show that it is also possible to measure the coherent vibrational SFG spectrum of the ethanol/air interface in this way. Our findings are useful for future far-UV or X-ray based nonlinear optical surface experiments on liquid jets. In addition, combined X-ray photoelectron spectroscopy and SHG/SFG measurements are feasible, which will be very useful in improving our understanding of the molecular foundations of electrostatic and chemical surface properties and phenomena. © 2014 AIP Publishing LLC. [http://dx.doi.org/10.1063/1.4896996]

I. INTRODUCTION

Liquid and aqueous interfaces in particular are intimately connected to many biological, chemical, and physical processes, such as protein folding and aggregation,[1,2] biological membrane formation,[3,4] catalysis,[5,6] emulsion, and aerosol processing.[7,8] Knowledge of the molecular surface structure is crucial for the understanding of these processes. Molecular level information of an interface can be obtained by using nonlinear surface spectroscopy. The two most common methods are Second Harmonic Generation (SHG) and Sum Frequency Generation (SFG) that were first applied to probing surfaces in 1969 by Brown and Matsuoka[9] and in 1987 by Guyot-Sionnest *et al.*,[10,11] and Harris *et al.*,[12] respectively. In a surface SHG or SFG experiment two intense electromagnetic fields from a pulsed laser source (two beams with identical, often near-infrared or visible frequency (SHG) or an infrared and visible pulse pair (SFG)) are reflected from an interface, where they induce a second-order polarization that oscillates at the second harmonic or sum frequency. The magnitude and spectral shape is determined by the second-order susceptibility tensor ($\chi^{(2)}$) of the material, which represents an averaged response of all molecular responses. Since $\chi^{(2)}$ is a physical property of the material, it must also reflect the spatial symmetry properties of that material (Neumann's principle). As a consequence, (in the electric-dipole approximation) $\chi^{(2)}$ vanishes in centrosymmetric bulk media.[13] This means that SHG and SFG can often be applied as surface sensitive techniques, with which only the first few molecular layers situated at the interface are probed. Vibrationally resonant SFG can be used to measure the coherent vibrational surface spectrum from the interface, which contains information about molecular composition, order, and chirality. Since the initial experiments, thousands of studies have been performed to elucidate the molecular complexity of a large variety of interfaces (reviewed in, e.g., Refs. 14–27). The most commonly employed geometry is the reflection geometry from a planar interface, but other geometries are also used. Scattering SHG or SFG, for example, can be used to probe the interfaces of micrometer and nanometer sized particles and droplets.[28,29] Such a geometry, aside from allowing access to the interface of small particles in buried liquid or solid media, also has advantages in decreasing the inherent challenges that are caused by chemical contaminations, which are present in every sample.[30] Scattering experiments thus form an attractive alternative for studying liquid/liquid interfaces.[31] Liquid jets are another alternative for reducing impurity induced artifacts[32,33] (as the interface is continuously refreshed) or avoiding the use of windows[34–36] when the optical excitation demands such applications. Heating effects are also eliminated in the liquid jet and it allows to study kinetics at interfaces.[37–39] Liquid jets are mostly used in X-ray photoelectron spectroscopy (XPS) and X-ray adsorption spectroscopy experiments[40–44] but have been used as well in kinetic resonant second harmonic experiments.[37] Recently, a microflow system based on a liquid microjet combined with a fluorescence microscope was employed to study interfacial reactions.[38,39] Cooling and freezing of bulk water in droplets have been studied using femtosecond X-ray spectroscopy on a liquid microjet.[45] Liquid microjets can also be used to study adsorption kinetics of surfactants on millisecond and
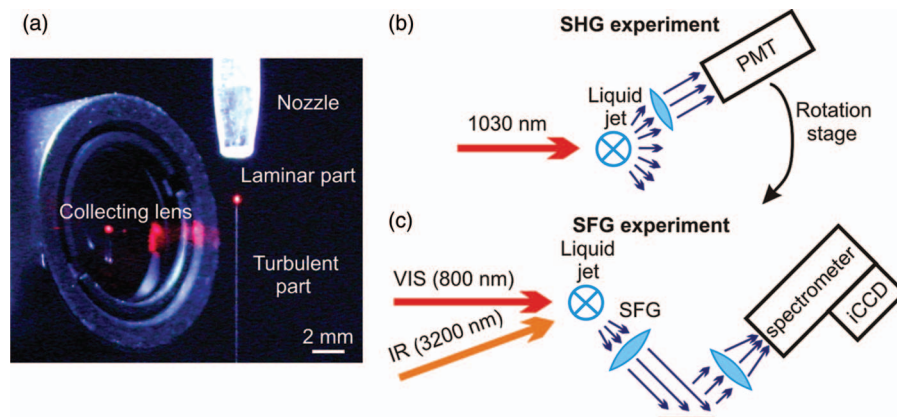
a)sylvie.roke@epfl.ch

FIG. 1.   Illustration of the experiments. (a) Photograph of the liquid microjet in operation next to the collecting lens of the SFG setup. The microjet is illuminated by a red diode laser at the boundary between the laminar flow (top, transparent) and turbulent (bottom, white) sections of the liquid microjet. (b) Schematic layout of the horizontal plane of the SHG experiment. (c) Schematic layout of the horizontal plane of the SFG experiment.

sub-millisecond timescales.[46–49] This is important for the investigation of stabilising foams, spreading of droplets on solid surfaces, inkjet printing, the coalescence of droplets and the breakup of jets. Furthermore, recent studies show that surface chemical equilibrium of water can be different with flow and without flow.[50]

Here, we explore the use of a liquid jet to perform non-resonant elastic second harmonic generation and vibrationally resonant sum frequency generation. We measure non-resonant SHG scattering patterns from the air/water interface of a microjet of pure water and observe a strong enhancement of the SHG signal for certain scattering angles. This enhancement can be explained by the optical properties and shape of the liquid microjet. SFG experiments at the surface of a liquid microjet of ethanol in air show that it is also possible to measure the coherent vibrational SFG spectrum of the ethanol/air interface. Based on our experiments, it should be possible in the future to use liquid jets to perform far-UV or X-ray based surface experiments employing SHG and SFG. In addition, combined X-ray photoelectron Spectroscopy and SHG/SFG measurements are feasible, which will be very useful in improving our understanding of the molecular foundations of electrostatic and chemical surface properties and phenomena.[51] In what follows, we first describe experimental details of the jet and the optical setups. Then we present SHG angular patterns from the liquid microjet and investigate the optical properties of the scattering geometry with ray optics. Finally, we present the results of the SFG experiments that were performed on a liquid microjet of ethanol.

II. EXPERIMENTAL PROCEDURES

A. Chemicals

Ethanol (99.9%) was purchased from Sigma-Aldrich. Ultra-purified, filtered and UV treated H_2O with an electrical resistance of at least 18.2 MΩ cm was obtained from a Milli-Q direct-Q-3UV system (Millipore, Inc.). For a typical measurement ~10 ml of liquid was needed.

B. The liquid jet

We used the liquid microjet setup described in Refs. 52 and 53. Briefly, this liquid jet source consists of an HPLC pump operating with a flow rate of 0.4 ml/min that is connected to a quartz nozzle (Microliquids GmbH) with an inner diameter of 35 μm. Pure water or ethanol was continuously pumped through an injection loop made of perfluoroalkoxyalkane (PFA) that is connected to a 2 μm inline PEEK filter that connects to the nozzle. The nozzle was mounted using an x-y-z translation stage (SmarAct piezo motors), such that the jet flow was vertical. The liquid flow is stable in air and remains intact for at least 2 mm downstream after exiting the nozzle. The jet eventually breaks up due to Rayleigh instabilities to yield aerosols. Consequently, the first 2 mm of the liquid flow is optically transparent (corresponding to laminar flow). Figure 1(a) shows a photograph of the liquid jet in operation.

C. The SHG setup

The system used for non-resonant SHG is described in detail in Ref. 54. Briefly, our experiments were performed using a pulsed Yb:KGW laser system (Pharos, Light Conversion) delivering 190 fs pulses centered at 1028 nm with a 200 kHz repetition rate. The laser power was set to 80 mW (as measured before the sample). A quarter-wave plate (Thorlabs, WPQ05M-1030), a half-wave plate (Thorlabs, WPH05M-1030), and a linear polarizer (Thorlabs, GT-10B) were used to control the polarization state of the incoming fundamental beam. A dichroic mirror (Thorlabs, M254H00) and a long pass filter (Thorlabs, FEL07500) were used to ensure that only 1028 nm light reached the sample. The thus filtered and polarized pulses were focused down to a 35 μm beam waist using a 7.5 cm plano-convex lens. The liquid jet was placed in the focus of the incoming beam. The scattered SHG light was collimated with a plano-convex lens (f = 5 cm) and subsequentially passed through an iris (to control the angular resolution), and a band pass filter (Chroma, ET525/50-2P, to separate the SHG signal from the fundamental). The filtered SHG

light was focused into a PMT with a plano-convex lens (f = 3 cm). Figure 1(b) shows a sketch of the setup. The gate width of the PMT was set to 10 ns, the acquisition time was 1.5 s, and 20 acquisitions were averaged for each data point. The PMT was mounted on a motorized rotation stage (Standa, 8MR151-1-670mA). The polarization of the scattered light was analyzed with a second polarizer (Thorlabs, GT-10A). The scattered SHG signal was measured with angular steps of 5° and an angular resolution of 3.5°.

D. The SFG setup

Broad-band vibrational sum frequency spectra were measured using the setup for sum frequency generation experiments described in Ref. 30. An 800 nm regeneratively amplified Ti:sapphire system (Spitfire Pro, Spectra physics) seeded with an 80 MHz 800 nm oscillator (Integral 50, Femtolasers) was operated at a 1 kHz repetition rate to pump a commercial OPG/OPA/DFG system (HE-TOPAS-C, Light Conversion), which was used to generate IR pulses. The visible beam was split off directly from the amplifier and spectrally shaped with a home-built pulse shaper. The angle between the 10 μJ visible (VIS) beam (800 nm, FWHM 15 cm^{-1}) and the 10 μJ IR beam (3200 nm, FWHM 163 cm^{-1}) was 20°. The SFG signal was detected at 45° with respect to the IR beam (see Fig. 1(c) for a sketch). The angular resolution was 22°. The SFG and VIS beams were polarized in the vertical (S) direction and the IR beam was polarized in the horizontal plane (P), leading to the polarization combination SSP. The recorded intensity was baseline subtracted and normalized by the SFG spectrum of a z-cut quartz crystal that was recorded before each measurement.

III. RESULTS AND DISCUSSION

We investigate the use of a liquid jet by measuring angular SHG intensity patterns in multiple polarization combinations and for different incident powers. SHG can originate from bulk water in the form of hyper Rayleigh scattering (HRS) as well as from the air/water interface. HRS is weak incoherent SHG that originates from the electronic non-centrosymmetry of isotropic liquid molecules.[55,56] The HRS intensity in the polarization combination SS is the strongest (approximately 8× stronger than the intensity in the PP combination) and the angular intensity is uniform.[57] In contrast, non-resonant SHG signal that is reflected from a water/air interface is strongly peaked around the phase-matched direction and is emitted preferentially in the PP polarization combination. Both HRS and surface SHG processes are characterized by a quadratic dependence on the incoming power.

A. The liquid jet as a micro-lens

Figure 2(a) shows typical SHG scattering patterns in PP and SS polarization combinations from a water jet. The PP signal displays two sharp peaks at ∼35° on top of two broader less intense peaks. The SS signal is also shown, which does not display much intensity. The shape of the pattern was the
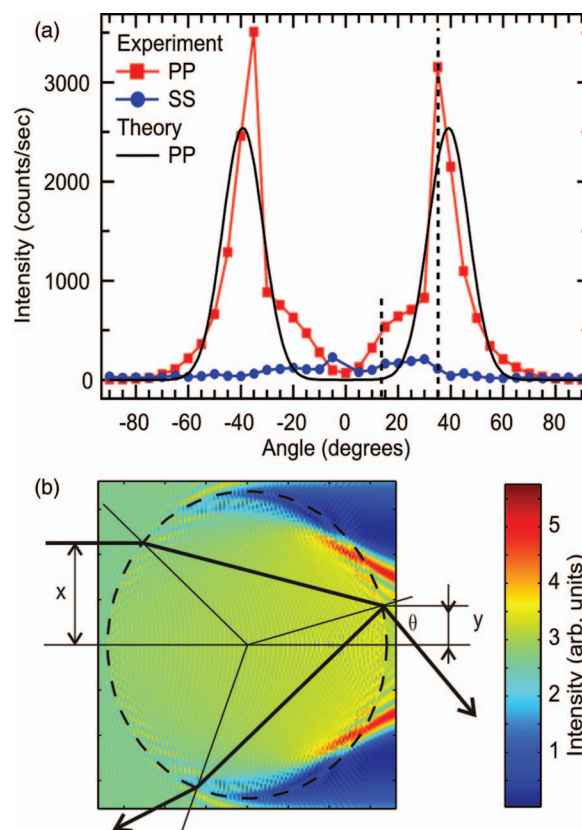

FIG. 2. Second harmonic generation from a water jet. (a) Scattering pattern from the laminar part of the liquid water jet. The polarization combinations were PP (red curve) and SS (blue curve). The dashed lines indicate the angles at which the power dependence measurements of Fig. 3 were performed. The black solid line shows two Gaussian peaks with an angular FWHM width of 18.2° centered at 39.2°, which represents the result of the considerations described in the text. (b) Linear Mie calculation of the electric field amplitude of the fundamental beam in P-polarization for a planar wave scattered from a cylinder of water. The drawing shows a scheme of refraction of one ray at the front and back side of the liquid jet.

same for the laminar and the turbulent parts of the liquid jet. It can be seen that the PP signal is 20× more intense than the SS signal. In addition, the maximum intensity of the PP SHG signal from the liquid jet is 15× larger than hyper-Rayleigh scattering in SS polarization from bulk water in the cuvette.[54] Given the difference between surface SHG and HRS, it is thus likely that the signal originates from the air/water interface and not from the bulk water. It is of further interest to note that the signal at 35° is ∼ 50× larger than the signal in the direction of the sum of the incoming wave vectors (phase matched direction, without refraction in the jet). In what follows we explain this behavior. For understanding the scattering pattern we use a simplified approach based on ray optics and Gaussian beam optics. We use Mie theory to qualitatively confirm our findings.

To explain the observed angular intensity pattern and to arrive at a reasonable estimate of the found curve, we first consider the intensity characteristics of the fundamental beam with ray optics[45] and Mie scattering,[58] and subsequently consider the resulting SH emission. A central parameter in ray optics is the distance of a ray that enters or exits the jet with respect to the optical axis (in the horizontal plane and

perpendicular to the optical axis). We assign this parameter with x for the entering beam and y for the emitted beam (see Fig. 2(b)). The jet can be modelled as a water cylinder with radius r and refractive index n. The relationship between x and y is given by

$$y = r \sin\left(2 \arcsin \frac{x}{nr} - \arcsin \frac{x}{r}\right). \qquad (1)$$

The emission or scattering angle θ is given by

$$\theta = 2\left(\arcsin \frac{x}{r} - \arcsin \frac{x}{nr}\right). \qquad (2)$$

The intensity of the fundamental beam I_ω at the back side of the cylinder can be expressed as a function of the incoming intensity:

$$I_\omega = I(x)\frac{dx}{dy}. \qquad (3)$$

It can be shown that this function goes to infinity at a scattering angle of $\theta = 39.2°$, which means that there will be strong focusing at the back of the cylinder. This angle agrees well with the maximum angle of Fig. 2(a). Our data, however, is not very sharply peaked as the above consideration suggests. Since the size of the "focus" at 39.2° is limited by diffraction effects it cannot be smaller than the fundamental wavelength (1.028 μm), so that the peaks in the angular pattern will be broadened. The actual size of the focus of the fundamental beam can be estimated more accurately by using linear Mie scattering theory. Fig. 2(b) shows the calculated E-field distribution for a plane wave of 1028 nm illuminating a water (n = 1.33) cylinder with a 35 μm diameter.[58]

At the back surface of the jet, the focused beam generates second harmonic photons in either reflection or transmission mode. Only the transmitted part reaches the detector. The reflected SHG light travels back through the liquid and then exits the jet in the direction of the incoming fundamental beam. The intensity of the transmitted second harmonic radiation can be written as:

$$I_{2\omega} \propto \chi^{(2)}_{eff} I_\omega^2, \qquad (4)$$

where $\chi^{(2)}_{eff}$ is the second-order susceptibility, which represents the response of the surface. For the polarization combination SS, the signal only relies on the $\chi^{(2)}_{y'y'y'}$ elements (with x', y', z' defined as a coordinate system with z' along the radially directed surface normal and x' along the azimuthal angle and y' along the symmetry axis of the cylinder). Since this element vanishes for isotropic surfaces,[27] Eq. (4) leads to $I_{2\omega} = 0$ for SS polarization. For the polarization combination PP, SHG signal arises from the elements $\chi^{(2)}_{z'z'z'}$; $\chi^{(2)}_{z'x'x'} = \chi^{(2)}_{z'y'y'}$; $\chi^{(2)}_{x'z'x'} = \chi^{(2)}_{y'z'y'}$; $\chi^{(2)}_{x'x'z'} = \chi^{(2)}_{y'y'z'}$, which are non-zero.

Assuming that our beams are Gaussian in shape, the broadening of the peaks in the angular pattern can be estimated. The divergence $\Delta\theta$ of the Gaussian SHG beam is given by $\Delta\theta = \frac{\lambda}{\pi b} = 18.2°$ where b is half the beam waist, i.e., $2b = 1.028$ μm and λ is the SH wavelength (514 nm). This estimated size of the area of the generated SH light is in agreement with theoretical values.[59] A normalized representation of $I_{2\omega}$ that consists of two Gaussian peaks centered around 39.2° and with a FWHM width of 18.2° is plotted in Fig. 2(a). This curve can be seen to capture the essentials
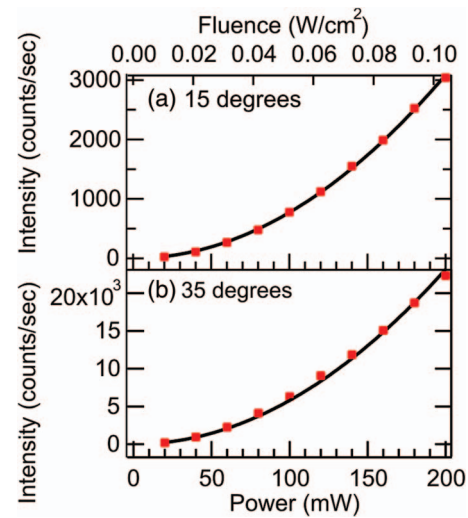

FIG. 3. Power dependence of the SHG intensity (data points) from the liquid jet of water for different scattering angles: $\theta = 15°$ (a) and $\theta = 35°$ (b). The iris size was 3 mm, corresponding to 3.5° angular resolution. The solid black line is a quadratic fit. The power was measured just before the beam hits the jet.

of the observed PP scattering pattern. Thus, the angular pattern can be explained by focusing of the incoming beam on the backside of the liquid jet in combination with subsequent surface second harmonic generation in transmission from the air/water interface. We note that this model is valid when the jet size (35 μm) is smaller or comparable with the fundamental beam waist (35 μm) and it is much larger than the wavelength (1.030 μm). Nonlinear Mie scattering theory can provide a more rigorous description of the angular pattern.[60]

In Fig. 2(a) the SH intensity at $\theta = 40°$ is much larger than the intensity that appears at $\theta = 0°$, i.e., the phase matching direction (without refraction in the jet). We can now see that this is caused by the focusing properties of the liquid jet that depend only on the wavelength, the shape of the jet, and the refractive index of the liquid. With such high intensities being generated at the backside of the liquid jet, it is valid to investigate to what extent this high intensity is damaging the material or altering its response. We have therefore measured the SHG response at two different scattering angles as a function of increasing incident pulse power. If there are no higher order effects or thermal lensing[61] we expect that the intensity scales quadratically with the incident power (P). Figure 3 displays the emitted SHG intensity for two different scattering angles that are highlighted with dashed lines in Fig. 2(a) ($\theta = 15°$ and $\theta = 35°$) versus the incoming power. The solid lines are fits to a quadratic power dependence. Since the data can be described well by a quadratic dependence, we conclude that there is little influence of the higher order processes on the signal. An explanation for this observation can be found by considering the beam size and the flow speed of the jet: The jet flows with 7 m/s (or 35 μm for every 5 μs, which is the interval between the laser pulses). Thus, for every new pulse (with a 35 μm beam waist at the front plane, and a focus of 2 μm in horizontal and 35 μm in vertical direction at the back plane) the interface is continuously refreshed. Thus, there is no sign of photodamage or changes in surface
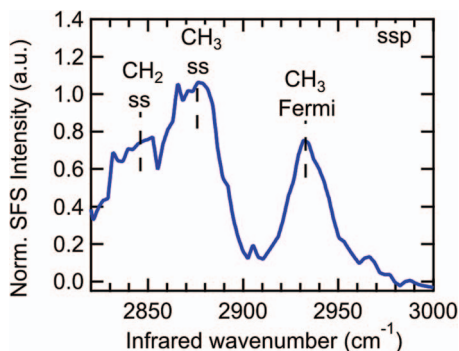
FIG. 4. SFG spectrum from the ethanol/air interface of a 35 μm liquid jet. The spectrum was averaged for 900 s.

structure due to laser induced heating[62] and one can use almost unlimited laser power.

B. SFG from a jet of ethanol

To test whether the observed intensity increase and angular dependence can also be exploited with sum frequency generation, we have performed an SFG experiment using a liquid microjet of ethanol (C_2H_5OH). Ethanol is an ideal reference solution because of its well-established spectral resonance in the 3 μm region of the IR spectrum (which was used in these experiments).[63] The experiment was performed in the geometry sketched in Fig. 1(c). Figure 4 shows the SFG spectrum recorded in the polarization combination SSP and acquired with an integration time of 900 s. The spectrum displays three resonances: The CH_3 Fermi resonance at 2940 cm^{-1}, the CH_3 symmetric stretch mode at 2875 cm^{-1}, and the CH_2 symmetric stretch mode at 2850 cm^{-1}. These resonances were also observed in SFG experiments from a planar ethanol/air interface.[63] Compared to Refs. 63 and 64, the spectrum in Fig. 4 has a larger symmetric CH_2 peak stretch mode. The difference can be explained either by slight differences in the chemical surface structure or by the difference in spectral resolution. As with the SHG experiments, no signal was recorded in the forward direction. Compared to the SHG data in Fig. 2 it does appear that the comparative enhancement of the signal is smaller for the SFG experiment. This can be explained by the difference in the wavelength of the two incoming beams: The 800 nm beam has a much narrower focus at the back plane of the jet ($\sim$1 μm) than the IR beam ($\sim$3 μm). This could in principle be improved by reshaping the beam size of the visible and IR beams so that they have the same size at the back plane of the jet. Nevertheless, Fig. 4 does show that it is possible to perform SFG experiments from the surface of a liquid jet. This opens up the possibility to incorporate liquid jets in X-ray or UV resonant SFG experiments that require a vacuum environment. It also means that comparative measurements can be performed with both XPS[51] and SHG or SFG, which will be beneficial in understanding the complex chemical nature of liquid interfaces.

One possible application of SHG/SFG on a liquid microjet is the study of adsorption kinetics occurring at a gas/liquid interface, similar to studies with an overflowing cylinder.[46–49]

Measurements on different vertical positions can be used here, but are limited by the stability of the laminar part of the microjet. To estimate the time resolution and duration of such a kinetic experiment we need to consider the length of the laminar part, the flow speed and the beam size. The flow speed in our setup was 7 m/s (but can be increased up to 70 m/s). The laminar length is approximately 2 mm, which results in a time window of 28–280 μs for 70–7 m/s, respectively. The size of focus is 35 μm in diameter, which means we can probe time intervals of $\Delta t = 0.5$–5 μs for 70 or 7 m/s, respectively.

IV. CONCLUSIONS

SFG and non-resonant SHG experiments were performed from the surface of a liquid microjet. We have measured non-resonant SHG scattering patterns from a water microjet and observe a strong enhancement of the SHG signal for certain scattering angles. We explain the enhancement by inserting the optical properties and shape of the liquid microjet in a ray optics computation that shows the fundamental beam is focused on the back side of the liquid jet (in the case that the jet and the beam have comparable dimensions). The resultant focused optical field produces SHG signal from the air/water surface that is peaked at an angle of $\sim$ 40° with respect to the optical axis. A polarization analysis shows that there is a negligible contribution of bulk processes. The power dependence shows that even up to very high laser powers the process remains second-order in nature, which is undoubtedly caused by the high refreshment rate of the jet surface. SFG experiments from the surface of a liquid microjet of ethanol in air show that it is also possible to measure the coherent vibrational spectrum of the ethanol/air interface in this way. In the future, it should be possible to use liquid jets to perform far-UV or X-ray based nonlinear optical surface experiments.[65] In addition, combined XPS/SHG/SFG measurements are feasible which will be very useful in understanding molecular foundations of electrostatic and chemical surface properties and phenomena.

[1]P. Ball, Chem. Rev. **108**, 74 (2008).
[2]D. Thirumalai, G. Reddy, and J. E. Straub, Acc. Chem. Res. **45**, 83 (2012).
[3]M. L. Berkowitz, D. L. Bostick, and S. Pandit, Chem. Rev. **106**, 1527 (2006).
[4]J. Milhaud, Biochim. Biophys. Acta, Biomembr. **1663**, 19 (2004).
[5]Y. Jung and R. A. Marcus, J. Am. Chem. Soc. **129**, 5492 (2007).
[6]R. N. Butler and A. G. Coyne, Chem. Rev. **110**, 6302 (2010).
[7]R. J. Buszek, J. S. Francisco, and J. M. Anglada, Int. Rev. Phys. Chem. **30**, 335 (2011).
[8]C. Solans, P. Izquierdo, J. Nolla, N. Azemar, and M. J. Garcia-Celma, Curr. Opin. Colloid Interface Sci. **10**, 102 (2005).
[9]F. Brown and M. Matsuoka, Phys. Rev. **185**, 985 (1969).

[10]P. Guyot-Sionnest, R. Superfine, J. H. Hunt, and Y. R. Shen, Chem. Phys. Lett. **144**, 1 (1988).

[11]J. H. Hunt, P. Guyot-Sionnest, and Y. R. Shen, Chem. Phys. Lett. **133**, 189 (1987).

[12]A. L. Harris, C. E. D. Chidsey, N. J. Levinos, and D. N. Loiacono, Chem. Phys. Lett. **141**, 350 (1987).

[13]P. Butcher, and D. Cotter, *The Elements of Nonlinear Optics* (Cambridge University Press, 1990).

[14]S. Roke, ChemPhysChem **10**, 1380 (2009).

[15]A. G. Lambert, P. B. Davies, and D. J. Neivandt, Appl. Spectrosc. Rev. **40**, 103 (2005).

[16]K. B. Eisenthal, Chem. Rev. **96**, 1343 (1996).

[17]G. Richmond, Annu. Rev. Phys. Chem. **52**, 357 (2001).

[18]G. L. Richmond, Chem. Rev. **102**, 2693 (2002).

[19]G. J. Simpson, ChemPhysChem **5**, 1301 (2004).

[20]M. A. Belkin and Y. R. Shen, Int. Rev. Phys. Chem. **24**, 257 (2005).

[21]M. J. Shultz, C. Schnitzer, D. Simonelli, and S. Baldelli, Int. Rev. Phys. Chem. **19**, 123 (2000).

[22]N. Bloembergen, Appl. Phys. B **68**, 289 (1999).

[23]C. D. Bain, J. Chem. Soc., Faraday Trans. **91**, 1281 (1995).

[24]Z. Chen, Y. R. Shen, and G. A. Somorjai, Annu. Rev. Phys. Chem. **53**, 437 (2002).

[25]H. Arnolds and M. Bonn, Surf. Sci. Rep. **65**, 45 (2010).

[26]Y. R. Shen, Proc. Natl. Acad. Sci. **93**, 12104 (1996).

[27]G. A. Reider and T. F. Heinz, in *Photonic Probes of Surfaces*, edited by P. Halevi (Elsevier, Amsterdam, 1995), p. 413.

[28]S. Roke and G. Gonella, Annu. Rev. Phys. Chem. **63**, 353 (2012).

[29]K. B. Eisenthal, Chem. Rev. **106**, 1462 (2006).

[30]R. Scheu, Y. Chen, M. Subinya, and S. Roke, J. Am. Chem. Soc. **135**, 19330 (2013).

[31]H. B. de Aguiar, J.-S. Samson, and S. Roke, Chem. Phys. Lett. **512**, 76 (2011).

[32]I. Jordan, A. Beloqui Redondo, M. A. Brown, D. Fodor, M. Staniuk, A. Kleibert, H. J. Worner, J. B. Giorgi, and J. A. van Bokhoven, Chem. Commun. **50**, 4242 (2014).

[33]M. A. Brown, N. Duyckaerts, A. B. Redondo, I. Jordan, F. Nolting, A. Kleibert, M. Ammann, H. J. Wörner, J. A. van Bokhoven, and Z. Abbas, Langmuir **29**, 5023 (2013).

[34]G. Gonella and H.-L. Dai, Langmuir **30**, 2588 (2014).

[35]S.-H. Jen, G. Gonella, and H.-L. Dai, J. Phys. Chem. A **113**, 4758 (2009).

[36]H. Wang, T. Troxler, A.-G. Yeh, and H.-L. Dai, Langmuir **16**, 2475 (2000).

[37]A. Castro, S. Ong, and K. B. Eisenthal, Chem. Phys. Lett. **163**, 412 (1989).

[38]T. Tokimoto, S. Tsukahara, and H. Watarai, Langmuir **21**, 1299 (2005).

[39]T. Tokimoto, S. Tsukahara, and H. Watarai, Chem. Lett. **30**, 204 (2001).

[40]M. Faubel, K. R. Siefermann, Y. Liu, and B. Abel, Acc. Chem. Res. **45**, 120 (2012).

[41]K. M. Lange, M. Soldatov, R. Golnak, M. Gotz, N. Engel, R. Könnecke, J.-E. Rubensson, and E. F. Aziz, Phys. Rev. B **85**, 155104 (2012).

[42]K. R. Wilson, B. S. Rude, T. Catalano, R. D. Schaller, J. G. Tobin, D. T. Co, and R. J. Saykally, J. Phys. Chem. B **105**, 3346 (2001).

[43]M. A. Brown, T. Huthwelker, A. Beloqui Redondo, M. Janousch, M. Faubel, C. A. Arrell, M. Scarongella, M. Chergui, and J. A. van Bokhoven, J. Phys. Chem. Lett. **3**, 231 (2012).

[44]M. A. Brown, I. Jordan, A. Beloqui Redondo, A. Kleibert, H. J. Wörner, and J. A. van Bokhoven, Surf. Sci. **610**, 1 (2013).

[45]J. A. Sellberg, C. Huang, T. A. McQueen, N. D. Loh, H. Laksmono, D. Schlesinger, R. G. Sierra, D. Nordlund, C. Y. Hampton, D. Starodub, D. P. DePonte, M. Beye, C. Chen, A. V. Martin, A. Barty, K. T. Wikfeldt, T. M. Weiss, C. Caronna, J. Feldkamp, L. B. Skinner, M. M. Seibert, M. Messerschmidt, G. J. Williams, S. Boutet, L. G. M. Pettersson, M. J. Bogan, and A. Nilsson, Nature **510**, 381 (2014).

[46]D. M. Colegate and C. D. Bain, Phys. Rev. Lett. **95**, 198302 (2005).

[47]R. A. Campbell, P. A. Ash, and C. D. Bain, Langmuir **23**, 3242 (2007).

[48]A. Angus-Smyth, R. A. Campbell, and C. D. Bain, Langmuir **28**, 12479 (2012).

[49]C. Yan, A. Angus-Smyth, and C. D. Bain, Faraday Discuss. **160**, 45 (2013).

[50]D. Lis, E. H. G. Backus, J. Hunger, S. H. Parekh, and M. Bonn, Science **344**, 1138 (2014).

[51]M. A. Brown, A. Beloqui Redondo, M. Sterrer, B. Winter, G. Pacchioni, Z. Abbas, and J. A. van Bokhoven, Nano Lett. **13**, 5403 (2013).

[52]M. A. Brown, F. Vila, M. Sterrer, S. Thürmer, B. Winter, M. Ammann, J. J. Rehr, and J. A. van Bokhoven, J. Phys. Chem. Lett. **3**, 1754 (2012).

[53]M. A. Brown, R. Seidel, S. Thurmer, M. Faubel, J. C. Hemminger, J. A. van Bokhoven, B. Winter, and M. Sterrer, Phys. Chem. Chem. Phys. **13**, 12720 (2011).

[54]N. Gomopoulos, C. Lütgebaucks, Q. Sun, C. Macias-Romero, and S. Roke, Opt. Express **21**, 815 (2013).

[55]R. W. Terhune, P. D. Maker, and C. M. Savage, Phys. Rev. Lett. **14**, 681 (1965).

[56]R. Bersohn, Y. H. Pao, and H. L. Frisch, J. Chem. Phys. **45**, 3184 (1966).

[57]B. Schürer, S. Wunderlich, C. Sauerbeck, U. Peschel, and W. Peukert, Phys. Rev. B **82**, 241404 (2010).

[58]R. F. Harrington, *Time-Harmonic Electromagnetic Fields* (IEEE Press, Piscataway, NJ, 2001).

[59]A. Rohrbach and W. Singer, J. Opt. Soc. Am. A **15**, 2651 (1998).

[60]A. G. F. de Beer and S. Roke, Phys. Rev. B **79**, 155420 (2009).

[61]R. D. Pyatt and D. P. Shelton, J. Chem. Phys. **114**, 9938 (2001).

[62]E. H. G. Backus, D. Bonn, S. Cantin, S. Roke, and M. Bonn, J. Phys. Chem. B **116**, 2703 (2012).

[63]L. Velarde and H.-F. Wang, Phys. Chem. Chem. Phys. **15**, 19970 (2013).

[64]H.-F. Wang, W. Gan, R. Lu, Y. Rao, and B.-H. Wu, Int. Rev. Phys. Chem. **24**, 191 (2005).

[65]T. E. Glover, D. M. Fritz, M. Cammarata, T. K. Allison, S. Coh, J. M. Feldkamp, H. Lemke, D. Zhu, Y. Feng, R. N. Coffee, M. Fuchs, S. Ghimire, J. Chen, S. Shwartz, D. A. Reis, S. E. Harris, and J. B. Hastings, Nature **488**, 603 (2012).